Research Square

Preprints are preliminary reports that have not undergone peer review.
They should not be considered conclusive, used to inform clinical practice,
or referenced by the media as validated information.

Paired Synthesis of Polycyclic Constitutional Isomers via Solvent-Controlled Skeletal Disproportionation

An-Xin Wu

chwuax@mail.ccnu.edu.cn

Central China Normal University https://orcid.org/0000-0001-7673-210X

Tong Lei

School of Chemistry and Chemical Engineering, Southeast University,

Chensen Xu

School of Chemistry and Chemical Engineering, Southeast University

Yi-Lin Liu

Southeast University

Min Zhang

Southeast University

Jia-Cheng He

Southeast University

Zhao-Rui Cao

Southeast University

Zhi-Xin Liao

School of Chemistry and Chemical Engineering, Southeast University,

Jia-Chen Xiang

Southeast University https://orcid.org/0000-0003-2422-6103

Article

Keywords:

Posted Date: November 18th, 2026

DOI: https://doi.org/10.21203/rs.3.rs-11713394/v1

License: This work is licensed under a Creative Commons Attribution 4.0 International License.
Read Full License

Additional Declarations: There is **NO** Competing Interest.

Paired Synthesis of Polycyclic Constitutional Isomers via Solvent-Controlled Skeletal Disproportionation

Authors: Tong Lei,[1] Chen-Sen Xu,[1] Yi-Lin Liu,[1] Min Zhang,[1] Jia-Cheng He,[1] Zhao-Rui Cao,[1] Zhi-Xin Liao,[1]* An-Xin Wu,[2,3]* and Jia-Chen Xiang[1]*

Affiliations:

1. School of Chemistry and Chemical Engineering, Southeast University, Nanjing 211189, P.R. China.
2. State Key Laboratory of Natural Product Chemistry, Lanzhou University, Lanzhou 730000, China.
3. Central China Normal University, Wuhan 430079, P.R. China.

Correspondence and requests for materials should be addressed to J-C. X (email: xiangjiachen@seu.edu.cn), A-X. W. (email: chwuax@mail.ccnu.edu.cn) and Z-X. L. (email: zxliao@seu.edu.cn)

Abstract: The paired synthesis of skeletally distinct polycyclic isomers has traditionally relied on separate and tailored synthetic designs, whereas their direct interconversion ranks among the most challenging transformations even within the realm of skeletal editing. However, we introduce that solvent-controlled skeletal disproportionation, despite its scarcity, offers a convenient means to formally achieve such atom-conserving skeletal reorganization. We exemplify this strategy with the copper-catalyzed aerobic oxidation of readily available diarylamines, arylglyoxals, and alkenes: the addition of a few drops of hexafluoroisopropanol (HFIP) to a 1,2-dichloroethane (DCE, 2.0 mL) suffice to trigger a complete selectivity flip in product skeletons. This “butterfly effect” leverages a switchable synthesis of two non-interconvertible, yet pharmaceutically privileged isomers—6/5/6/6 tetracyclic indolo[1,2-*a*]quinolines and 6/6 semi-saturated 2-acyl-1,4-dihydroquinolines, whose structural divergence is quantified by an average Tanimoto coefficient of 0.45. DFT calculations reveal that HFIP resolves the inherent regioselectivity conundrum between electron-rich arylamines and dicarbonyl electrophiles by reshaping the ring-size of competing transition states through hydrogen bonding, thereby redirecting chemoselectivity at the onset of the domino process. Biological evaluation across three cancer cell lines shows that this solvent-controlled skeletal divergence directly yields pronounced bioactivity bifurcation between the two isomers. This strategy allows the parallel expansion of compound libraries and would accelerate biological evaluation through a single synthetic design.

Introduction

The past years have witnessed remarkable progress in first-degree (1°) scaffold hopping through skeletal editing, which focuses on heterocycle replacement.[1-5] In sharp contrast, synthetic strategies for fourth-degree (4°) scaffold hopping[6-9]—a topology- or shape-level overhaul of the core skeleton with minimal perturbation of pendant groups—remain largely underdeveloped. Polycyclic scaffolds and their core-distinct constitutional isomers represent privileged targets for medicinal research especially 4° scaffold hopping studies, as they share identical elemental composition, molecular weight, and closely related pendant groups (Figure 1A).[10,11] For example, Sheng and co-workers reported that indolopyrazinoquinazolinone, a constitutional isomer of evodiamine bearing a distinct core skeleton (Figure 1B), exhibited more than four-fold higher inhibitory activity against the HCT116 cell line. Further peripheral modification of this post-hopping scaffold enhanced the activity by over 20,000-fold, a level

unattainable on the pre-hopping scaffold bearing the same peripheral substituents.[12] Despite such promise, systematic investigation of activity differences and structure-activity relationships for constitutional isomer pairs with entirely distinct ring systems and 3D shape remains elusive and often precluded by a fundamental synthetic burden: pre- and post-hopping isomers typically require separate and tailored routes from different starting materials. Given that constitutional isomerization of such structurally robust isomeric architectures is chemically formidable, a diversity-generating tactic that enables selective access to skeletally distinct polycyclic isomers from identical starting materials remains highly desirable[13-15].

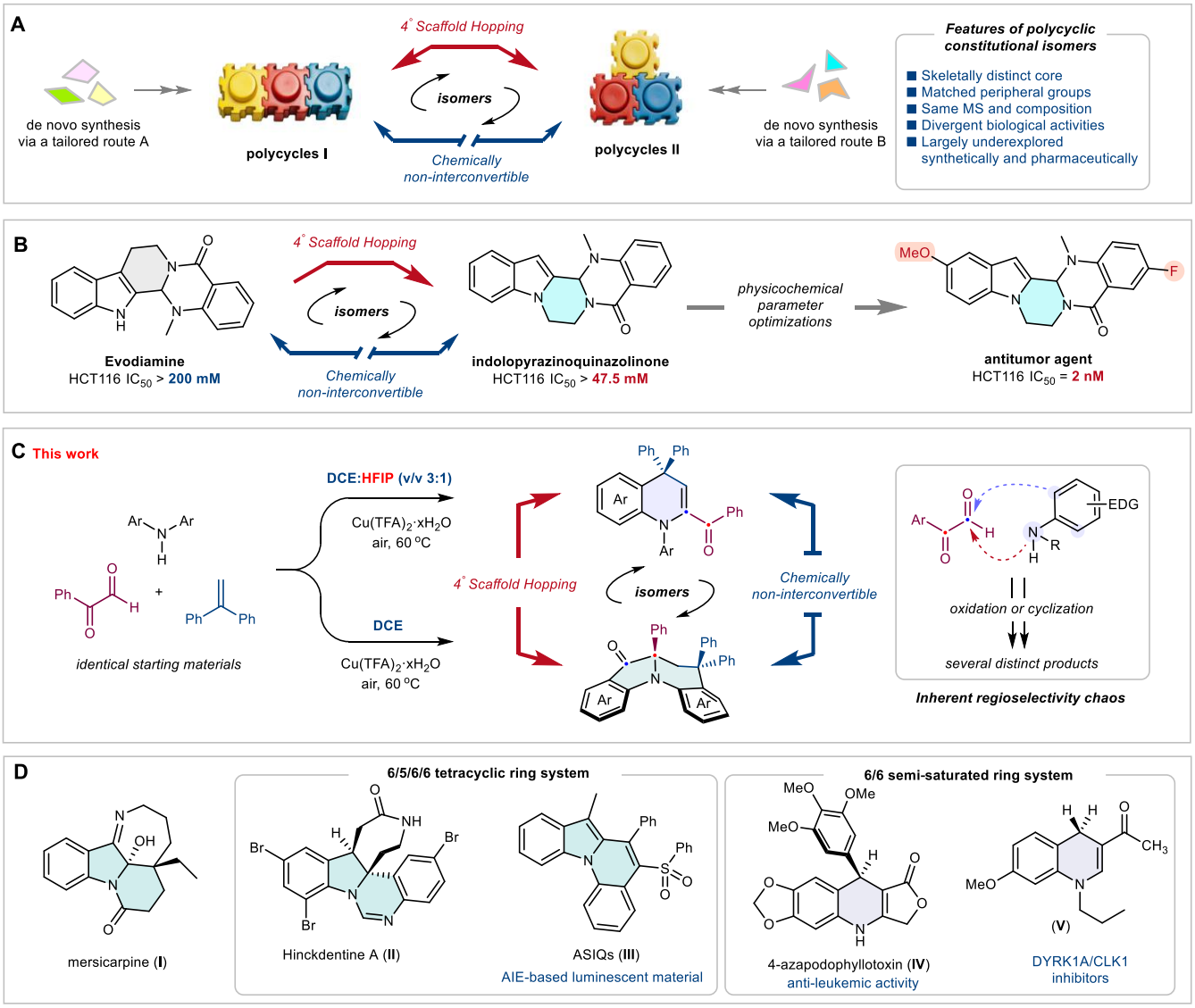


Figure 1 | Brief Introduction of 4° scaffold hopping between two polycyclic constitutional isomers (A, B) and our synthetic hypothesis on solvent-controlled skeletal disproportionation (C, D)

Solvent effects offer a powerful and operationally simple means for product diversification. However, solvent-controlled skeletal divergence—where the core framework itself is altered—remains exceptionally rare, especially when contrasted with the well-established roles of solvents in modulating stereoselectivity[16,17], regioselectivity[18-21], or serving as reactants[22-24]. In these later cases, solvent effects operate late in the domino sequence, after the core skeleton is fixed, giving only peripheral diversity[25-27] and often interconvertible products[28-33]. By contrast, we reasoned that early-stage solvent intervention could redirect the pathway from the outset, leading to stark skeletal divergence. This strategy, though rarely demonstrated, would enable the convenient, paired synthesis of skeletally

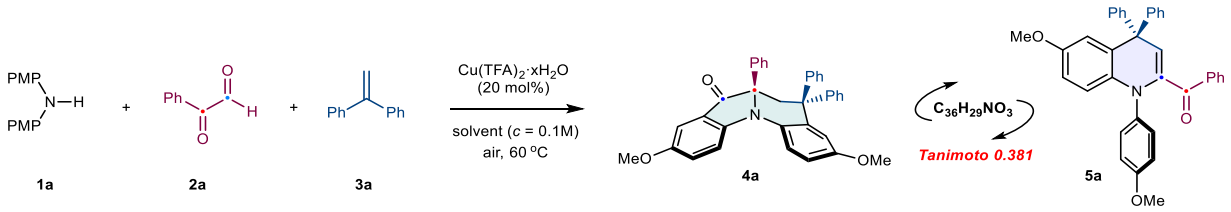
distinct constitutional isomers from identical starting materials, allowing parallel exploration of their chemical space. Two precedents exist, both in monocyclic systems: Barluenga's solvent/temperature-controlled cyclopentene synthesis[35,36] and Leonori's solvent-switchable thiazole/isothiazole photochemistry[37]. Despite these pioneering reports, achieving polycyclic isomers—a class of even greater importance in medicinal chemistry[11]—with pronounced scaffold diversification through simple solvent switching remains counterintuitive.

Building on our interest in arylglyoxal-involved scaffold hopping processes,[38] we noted that the regioselective competition between the *N* and *C* nucleophilic sites of arylamines in their reaction with multi-carbonyl electrophiles—the very first step of the domino sequence—remains a long-standing challenge in arylglyoxal chemistry. We recognized that addressing this conundrum could provide a suitable design platform for the skeletal bifurcating synthesis we sought. Accordingly, we developed a three-component reaction of diarylamines, arylglyoxals, and alkene trapping agent[39] under copper-catalyzed aerobic conditions, enabling solvent-switched synthesis of two skeletally novel, non-interconvertible polycycles—indolo[1,2-*a*]quinolines (**4**)[40-51] and 2-acyl-1,4-dihydroquinolines (**5**) [52-61]—which represent a pair of constitutional isomers featuring distinct 3D fused ring systems (Figure 1C, D).

Results

Synthesis of indolo[1,2-*a*]quinolines and 2-acyl1,4-di-hydroquinolines. Bis(4-methoxyphenyl)amine (**1a**), phenylglyoxal (**2a**) and 1,1-diphenylethylene (**3a**) were submitted as model substrates to copper-catalyzed aerobic oxidations (Table 1).[62,63] When dichloroethane (DCE) was used as the solvent, the optimal reaction temperature was determined to be 60°C, providing indolo[1,2-a]quinoline **4a** in 88% yield (entries 1-2). We only detected a little amount of competitive 2-aryl-1,4-dihydroquinoline product **5a**. When the reaction was conducted in a mixed solvent of DCE and hexafluoroisopropanol (HFIP) (v/v 3:1), **4a** was scarcely detectable. Instead, **5a** was obtained as the major product in 89% yield (entry 3). Considering that the dielectric constants of HFIP and DCE are not dramatically different (ε 15.7 vs 10.4), hydrogen-bonding interactions were proposed to be responsible for the observed selectivity. Further use of methanol, ethanol, as a substitute for HFIP resulted in low conversion, yielding neither **4a** nor **5a** (entries 4-5). Methyl tert-butyl ether (MTBE) show ineffective to the conversion (entry 6), while diethylene glycol diethyl ether (DEE) exhibits equivalent efficacy as HFIP in terms of reaction selectivity, though the yield of **5a** is reduced (entry 7). When HFIP is used as sole solvent, **5a** was the only product. Given the intrinsic acidity of HFIP (pK_a 9.3), we attempted to replace it with other acidic additives. However, neither acetic acid nor trifluoroacetic acid (TFA) promoted the formation of **5a**; moreover, the yield of **4a** dropped significantly when a strong acid (TFA) was used (entries 10). We attribute this negative outcome to the protonation-induced deactivation of the NH nucleophile. Finally, we used the conditions from entry 2 and entry 3 as the optimized ones for synthesizing **4a** and **5a**, respectively. These two sets of conditions are identical (copper salt, equivalent, concentration, temperature) except that the latter adds HFIP, resulting in a pair of constitutional isomers with the molecular formula $C_{36}H_{29}NO_3$, whose structural divergence is quantified by a Tanimoto coefficient of 0.381. We noted that **4** represents a previously undescribed structure, whereas the synthetic approach towards 2-acyl-1,4-dihydroquinolines **5** has not been reported to date.

Table 1 | Screening of reaction conditions.[a]



Entry	Solvent (v/v)	Additives	Yield of **4a** (%)[b]	Yield of **5a** (%)[b]
1	DCE at 40 °C	-	30%	trace
2	DCE	-	**88%**	~5%
3	DCE : HFIP (3:1)	-	trace	**89%**
4	DCE : MeOH (3:1)	-	trace	trace
5	DCE : EtOH (3:1)	-	trace	trace
6	DCE : MTBE (3:1)	-	trace	trace
7	DCE : DEE (3:1)	-	trace	48%
8	HFIP	-	trace	88%
9	DCE	AcOH (1.0 equiv)	85%	trace
10	DCE	TFA (1.0 equiv)	~10%	~10%

[a]Reaction conditions: **1a** (0.2 mmol), **2a** (0.4 mmol), **3a** (0.4 mmol), $Cu(TFA)_2 \cdot xH_2O$ (0.04 mmol) in solvent (2.0 mL, c 0.1 M) at 60 °C for 5 h. [b]Isolated yield.

To validate the capability of our solvent-controlled skeletal disproportionation in accessing constitutional isomers in a pairwise fashion, we conducted substrate scope studies using identical starting materials for both the **4** and **5** series (Figure 2). Arylglyoxals bearing 3-trifluoromethoxy (**4b** and **5b**), 4-methyl (**4c** and **5c**), or 2-naphthyl groups (**4e** and **5e**) all proceeded smoothly to afford both two heterocyclic scaffolds in high selectivity. In general, the yields of the 2-acyl-1,4-dihydroquinolines (series **5**) were slightly lower than those of the indolo[1,2-*a*]quinolines (series **4**). In addition, 1,1-disubstituted (**4d** and **5d**) and 1,2-disubstituted (**4f** and **5f**) alkenes afforded the corresponding isomeric pairs in moderate to good yields. Notably, the reaction using 9-methylene-9H-fluorene delivered a pair of spiro-fused polycyclic architectures (**4g** and **5g**). Likewise, simultaneous variation of both substrates **1** and **2** delivered the corresponding isomers in comparable yields (**4h** and **5h**). Moreover, substrates bearing pre-installed drug motifs, such as thymol (**4i** and **5i**), Hydronopol (**4j** and **5j**), Ciprofibrate (**4k** and **5k**) were converted to the target product pairs, thereby enabling the parallel investigation of activity differences among drug fragments incorporating distinct pharmacophores. These examples illustrate that our acidic reaction conditions are compatible with ester groups, ether groups and dichlorocyclopropane moieties. The scale-up reactions performed on a 3.0 mmol scale afforded **4a** in 62% yield and **5a** in 57% yield. Overall, this synthetic approach displays good substrate scope and functional group compatibility for the parallel construction of polycyclic isomers with high selectivity and closely matched yields.

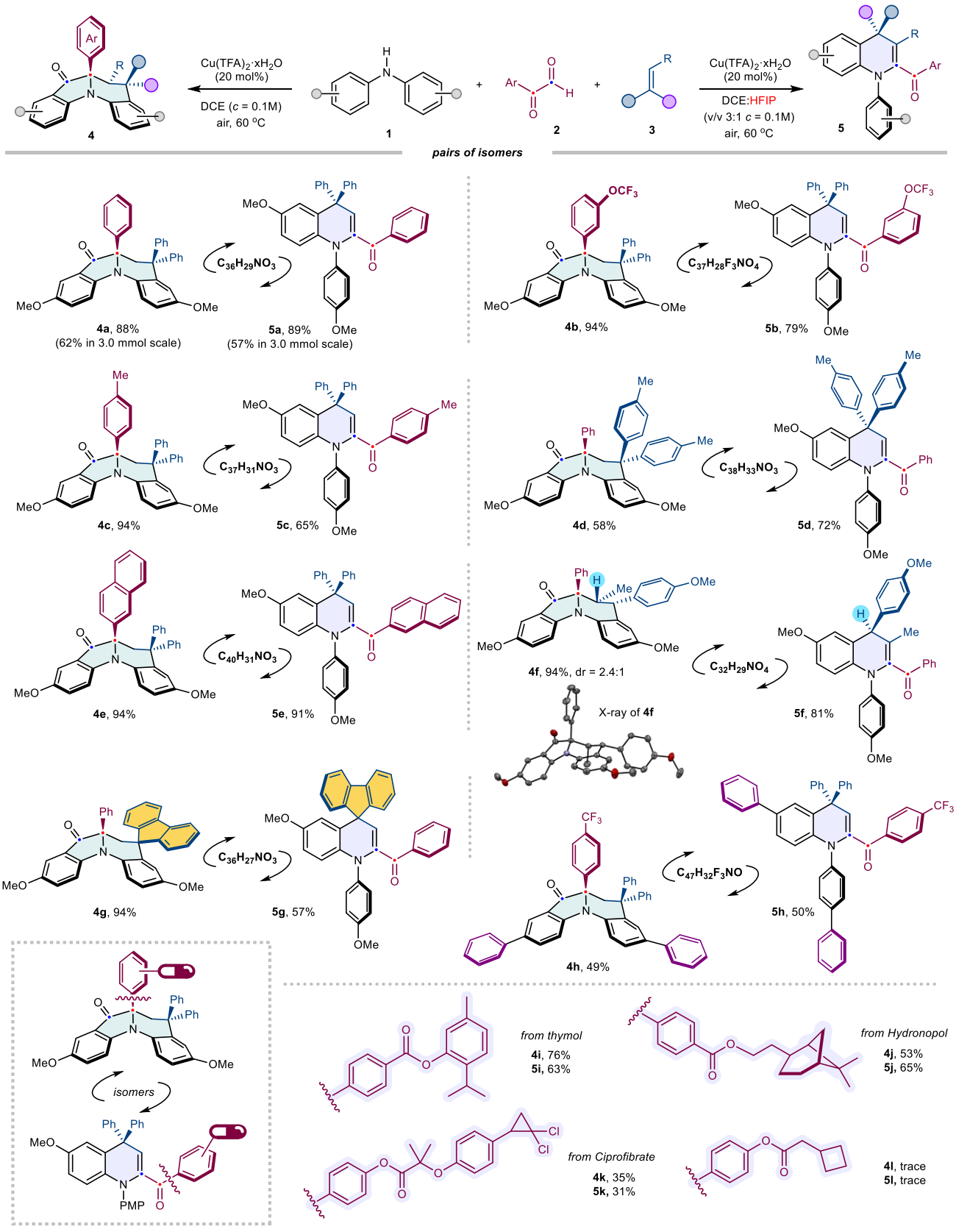


Figure 2 | Reaction scope for the synthesis of indolo[1,2-a]quinoline 4. [a]General conditions: **1a** (0.20 mmol), **2a** (0.4 mmol), **3a** (0.4 mmol), $Cu(TFA)_2 \cdot xH_2O$ (0.04 mmol) in a mixed solvent of DCE (2.0 mL) at 60 °C. Isolated yield. Reaction scope for the synthesis of 2-acyl-1,4-dihydroquinolines **5**. [a]General conditions: **1a** (0.20 mmol), **2a** (0.4 mmol), **3a** (0.4 mmol), $Cu(TFA)_2 \cdot xH_2O$ (0.04 mmol) in a mixed solvent of DCE (1.5 mL) and HFIP (0.5 mL) at 60 °C. Isolated yield.

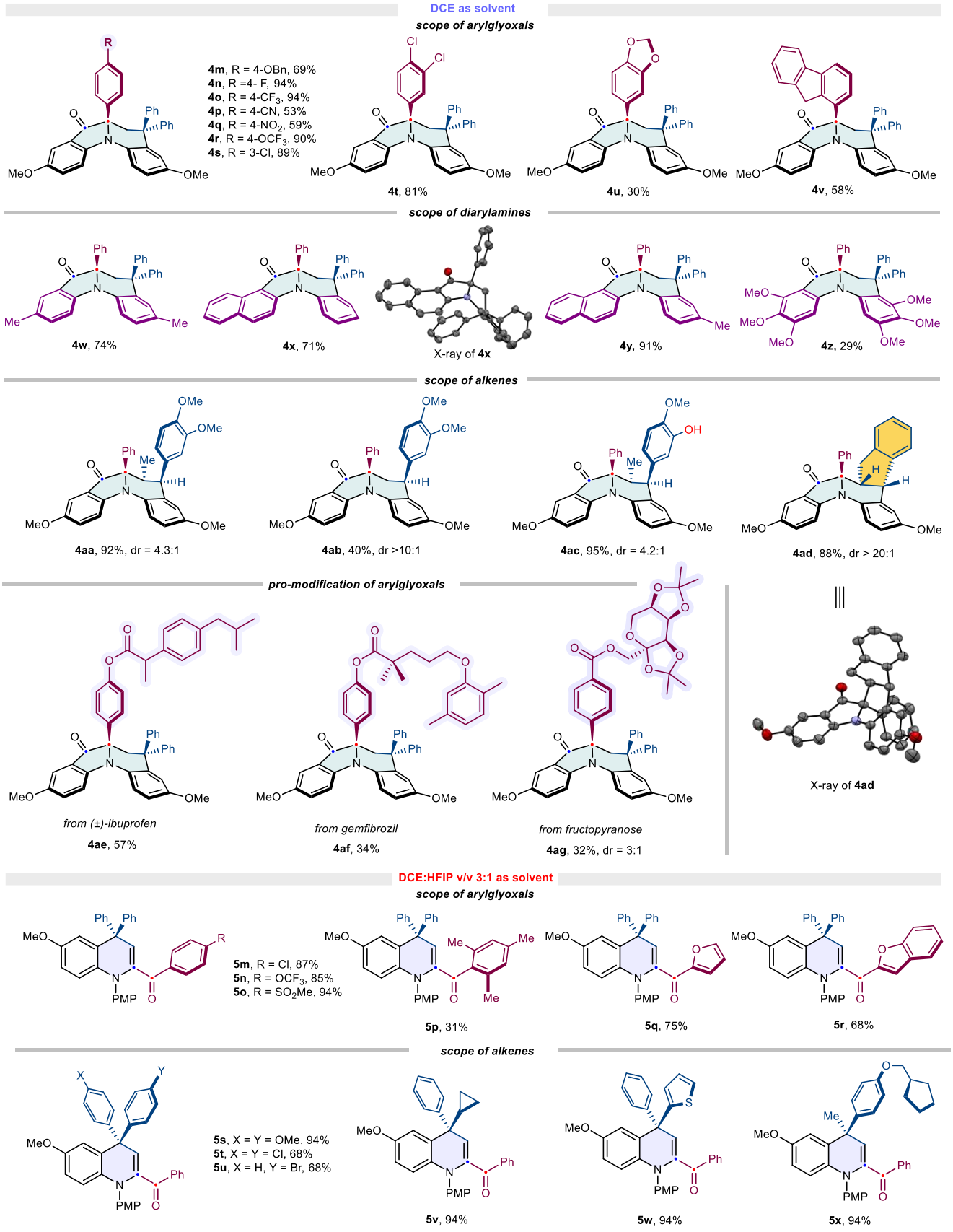
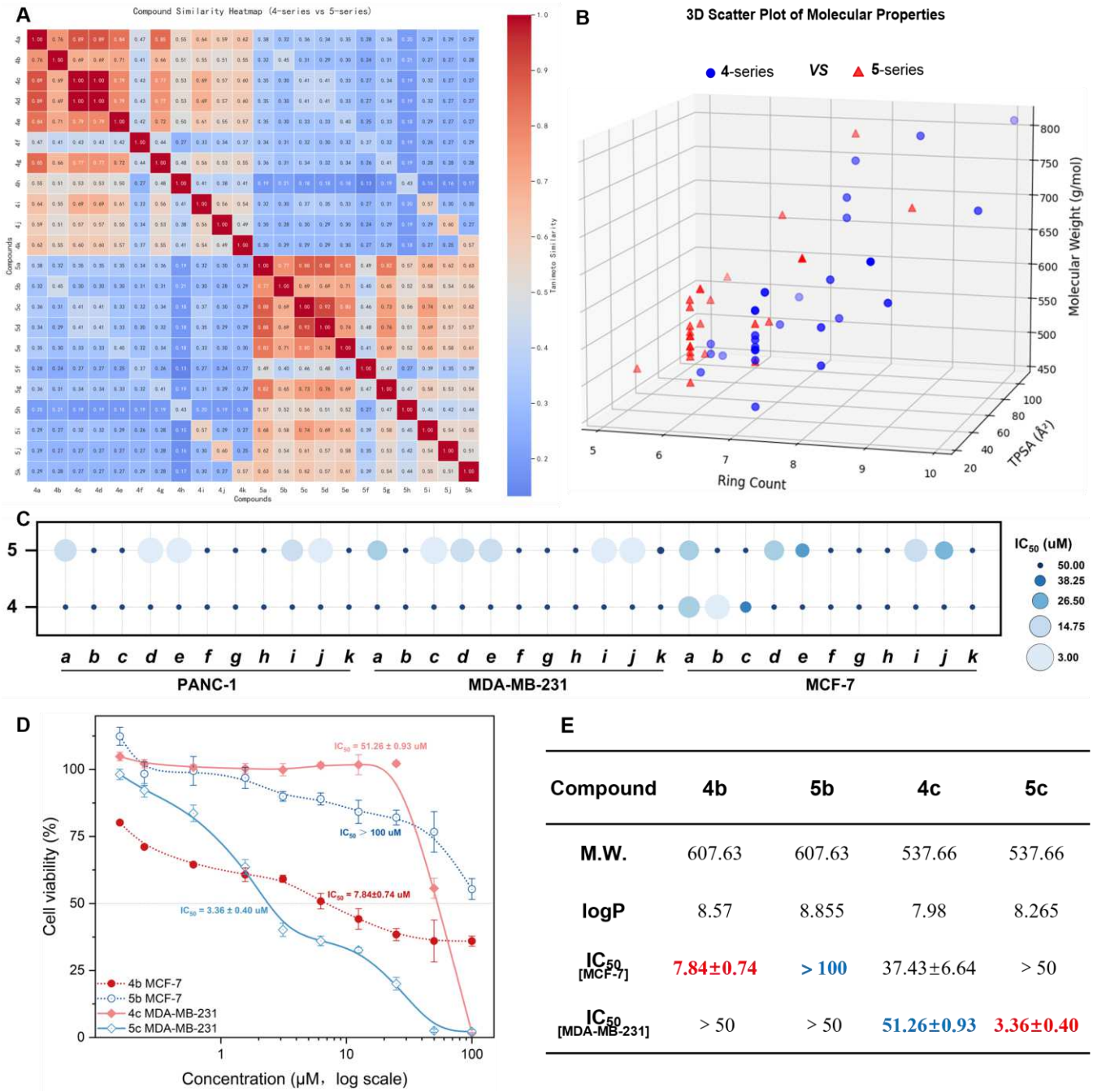


Figure 3 | Reaction scope for the synthesis of indolo[1,2-a]quinoline **4**. [a]General conditions: **1a** (0.20 mmol), **2a** (0.4 mmol), **3a** (0.4 mmol), $Cu(TFA)_2 \cdot xH_2O$ (0.04 mmol) in asolvent of DCE (2.0 mL) at 60 °C. Isolated yield. Reaction scope for the synthesis of 2-acyl-1,4-dihydroquinolines **5**. [a]General conditions: **1a** (0.20 mmol), **2a** (0.4 mmol), **3a** (0.4 mmol), $Cu(TFA)_2 \cdot xH_2O$ (0.04 mmol) in a mixed solvent of DCE (1.5 mL) and HFIP (0.5 mL) at 60 °C. Isolated yield.



E

Compound	4b	5b	4c	5c
M.W.	607.63	607.63	537.66	537.66
logP	8.57	8.855	7.98	8.265
IC_{50} [MCF-7]	7.84±0.74	> 100	37.43±6.64	> 50
IC_{50} [MDA-MB-231]	> 50	> 50	51.26±0.93	3.36±0.40

Figure 4 | (A) Compound similarity heatmap of the isomeric products. (B) 3D Scatter plot for all the synthetic products. (C) Antiproliferative activities of **4a-k** and **5a-k** against PANC-1, MDA-MB-231, and MCF-7 cells. (D) The concentration-viability curves of **4b**, **5b**, **4c**, **5c**. (E) Divergent bioactivity profiles between series **4b**, **c** and **5b**, **c** in antitumor activity (μM).

To further explore the peripheral generality, we next tested the substrate scope for indolo[1,2-*a*]quinoline products (Figure 3). A series of arylglyoxals bearing diverse substituents on the aromatic ring were smoothly converted into the desired products in moderate to good yields. The compatible substituents included benzyloxy, halogens, trifluoromethyl, and nitro groups at different positions of the benzene ring (**4m-u**). In general, substrates with electron-donating groups on the aryl part diminished yields (**4m**, **4u**). Furthermore, arylglyoxal bearing steric hindrance substituent, such as 9H-fluoren-1-yl (**4v**) group, is a suitable substrate candidate. Regarding the diarylamine, di-p-tolylamine (**4w**) and N-phenylnaphthalen-2-amines (**4x**, **4y**) proved effective for the transformation. The regioselectivity observed with **4x** and **4y** is attributed to the higher π-nucleophilicity of the naphthalene ring relative to the

N-phenyl ring toward the carbonyl electrophile. Substitution with methoxy groups at the 3, 4, and 5 positions of the aromatic ring resulted in an unsatisfactory outcome, providing the target product **4z** in only 29% yield. However, simple diphenylamine or diarylamines bearing electron-withdrawing groups failed to afford the desired product.

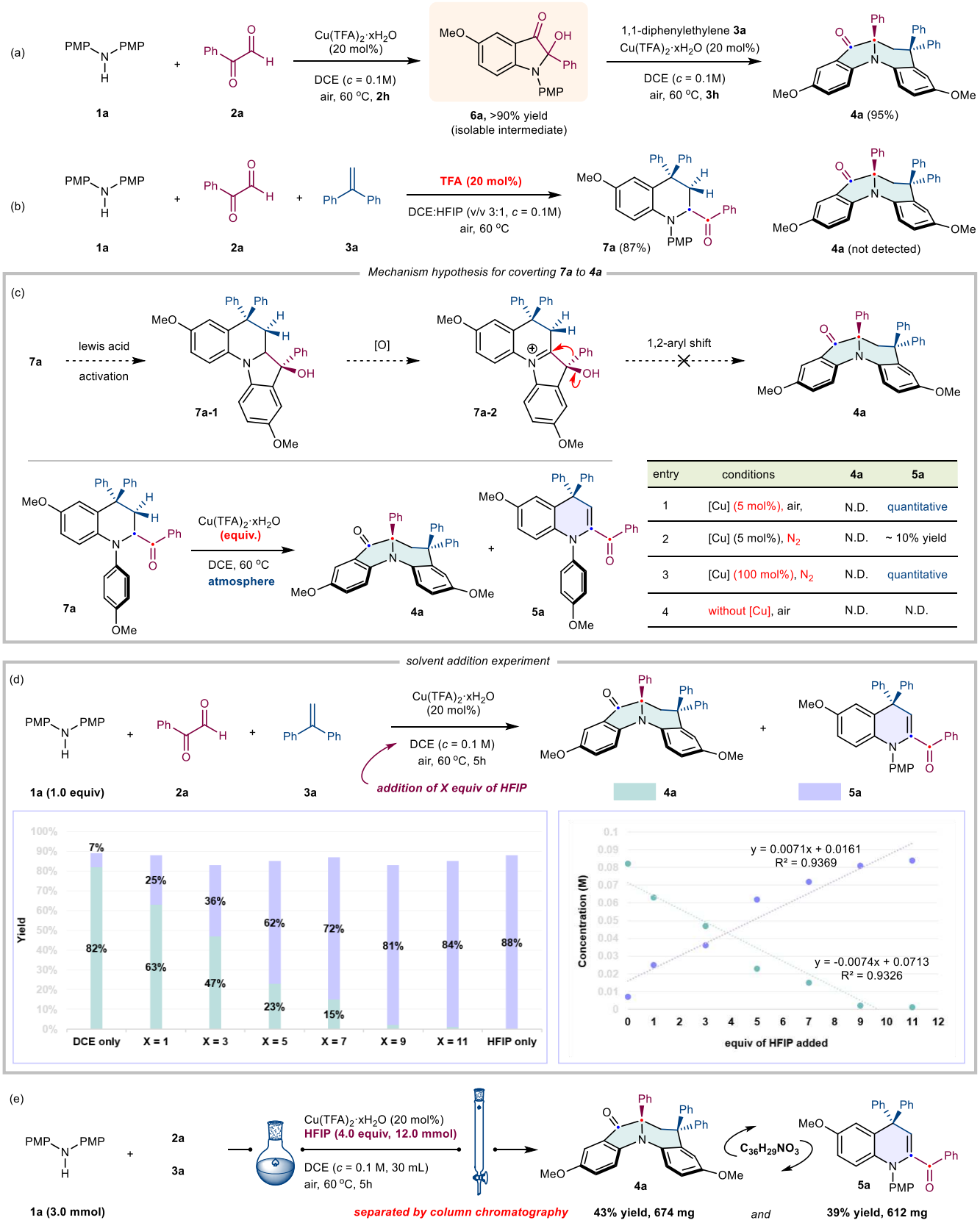


Figure 5 | Controlled experiments (a-d) and scale-up reaction afforded isomeric products in parallel from one-pot protocol (e).

To our delight, various alkene substrates demonstrated high diversity. The scope includes 1,1-disubstituted, 1,2-disubstituted, and mono-substituted alkenes. Styrene derivatives with electron-donating substituents (**4aa**) or simple styrenes (**4ab**) all participated successfully, even a phenolic hydroxy group was tolerated (**4ac**). A densely packed polycyclic framework (**4ad**) with excellent diastereoselectivity was efficiently produced using 1*H*-indene as the substrate. We also encountered limitations regarding the alkene scope. Alkenes bearing electron-withdrawing groups (e.g., methyl cinnamate, methyl acrylate) or non-activated aliphatic alkenes failed to afford the desired product. These limitations suggest that the mechanism may proceed through a cationic pathway. Moreover, arylglyoxals bearing pre-installed drug motifs, such as ibuprofen (**4ae**), gemfibrozil (**4af**) and fructopyranose (**4ag**) were converted to the target products, highlighting the substrate compatibility.

When the mixed solvent of DCE and HFIP (v/v 3:1) was employed, the product selectivity switched to afford 2-aryl-1,4-dihydroquinolines (**5**) completely as we expected. A range of arylglyoxals, including those bearing trifluoromethoxy (**5n**), dimethylsulfoxonyl (**5o**) or heteroaromatic substituents (**5q, 5r**), proceeded smoothly in these conditions (Figure 3). Notably, when 2,4,6-trimethylbenzyl glyoxal was used, a reduced yield was obtained, which may be attribute to the steric hindrance (**5p**). A variety of alkenes with different substitution patterns were then subjected to the reaction. 1,1-Diaryl-disubstituted terminal alkenes (**5s**-**5u**), even containing a 4-chloride substituent (**5t**) were compatible substrates. Furthermore, unsymmetrical alkenes bearing cyclopropyl (**5v**) or thienyl (**5w**) groups afford desired products in high yields. Furthermore, electron-rich 1,2-disubstituted alkene participated in the reaction smoothly, resulting in 2-aryl-3-substituted 1,4-dihydroquinolines (**5x**). Under these conditions, the formation of **4** was fully suppressed across all substrates examined.

The heatmap separates the compounds into two distinct clusters (Figure 4A): the **4**-series (top-left) and the **5**-series (bottom-right). Within each cluster, high similarity values (e.g., **4a**/**4c** = 0.89) indicate a shared core scaffold, whereas the low cross-series similarities (average 0.45) confirm that the two series are constitutional isomers with distinct core skeletons. Cross-cluster similarities are generally low (<0.4), with most pairs falling below 0.2, reflecting divergence in both core and periphery. Consider compound **4h** as an example. Its similarities to the majority of **5**-series members are low (<0.2). However, the **4h**/**5h** pair gives a similarity of 0.43—still modest but notably higher than typical cross-series values. Meanwhile, within the **4-**series, **4h** shows an unusually low similarity of only 0.27 with **4f**, compared to the generally high intra-series values. These observations confirm the clear segregation of the two families and highlight the rich structural diversity among individual members within each series. Furthermore, 3D scatter plot (Figure 4B) maps all 58 synthetic products across ring count, TPSA, and molecular weight. The **4**-series is enriched with higher ring counts (7.0–10.0) and exhibits a gradual increase in molecular weight with ring count, consistent with their more polycyclic structures. The **5**-series centers on lower ring counts (5.0–7.0) with a wider variance in molecular weight, reflecting their unique and divergent core architecture. The well-separated domains confirm successful divergence into two unique core scaffolds, while the wide dispersion of data points demonstrates high structural diversity across the entire library.

Indolo[1,2-a]quinolines and 1,4-dihydroquinolines have been reported to exhibit antiproliferative activity against MCF-7 and MDA-MB-231 cells[42] or antileukemic activity[52], respectively. However, how these two types of constitutional isomers differ in their biological activities remains unclear and prompted our interest. We therefore evaluated the antiproliferative activities of the 11 pairs of isomers (**4a**–**k** and **5a**–**k**) against three human cancer cell lines—PANC-1 (pancreatic cancer), MDA-MB-231 (triple-negative breast cancer), and MCF-7 (hormone-dependent breast cancer)—using the CCK-8 assay. Across all three cell lines, the **5**-series exhibited markedly

stronger and broader cytotoxicity than the **4**-series. For instance, all **4**-isomers were essentially inactive against PANC-1 and MDA-MB-231 (IC_{50} > 50 μM), whereas multiple **5**-isomers achieved low-micromolar potency. Even on MCF-7 cells, the **5**-series generally displayed a higher number of active compounds (e.g., **5i**: 11.82 μM, **5d**: 18.61 μM) (Figure 4C). These results demonstrated that the simple addition of HFIP successfully enables a fourth-degree (4°) scaffold hopping. Moreover, constitutional isomers with identical molecular weights and related pendant groups can exhibit markedly different activities solely due to their core skeletons. For instance, **4b** potently inhibited MCF-7 cells (IC_{50} = 7.84 μM), while **5b** was inactive (>100 μM). Conversely, **5c** showed strong activity against MDA-MB-231 cells (IC_{50} = 3.36 μM), whereas **4c** was only weakly active (51.26 μM) (Figure 4D,E).Thus, these results clearly demonstrate that the scaffold divergent synthesis of polycyclic constitutional isomers can directly result in their bioactivity bifurcation. Accordingly, this synthetic strategy offers a convenient means to explore diverse bioactivity space in parallel.

Control experiments and mechanistic considerations. Next, control experiments were conducted to explore the reaction mechanism. Treated **1a** with **2a** for 2 hours under standard conditions, **3a** was then submitted, regardless of whether DCE or DCE and HFIP (v/v = 3:1) was used, **4a** was selectively obtained in quantitative yield. In the first stage of this reaction, the separable intermediate was identified as 2-hydroxy-indol-3-one **6a** (Figure 5-a). When TEMPO was added to the model reaction used to produce **4a**, the conversion was completely muted. A radical process, originating from the interaction between copper salts and oxygen, may be involved in our transformation. Upon replacing the copper salt with TFA, we obtained the [4+2] adduct **7a** in high yield regardless of whether DCE or DCE and HFIP (v/v = 3:1) was used (Figure 5-b). Mechanistically, **7a** can be activated by a Lewis acid to undergo cyclization, affording **7a-1**. This intermediate can then be oxidized to the iminium **7a-2**, which undergoes a 1,2-aryl migration to furnish **4a** (Figure 5-c). However, this proposed mechanism was completely refuted by further control experiments. In the presence of 5 mol% copper salt and oxygen, **7a** was fully converted to **5a** without the formation of **4a** (Figure 5-c entry 1). This process was subsequently proved to be accomplished via copper-catalyzed aerobic oxidation (Figure 5-c entries 2-4). Under our standard conditions, 24 equivalents of HFIP (relative to **1a**) are used (0.5 mL). To probe the solvent effect, we varied the dose of HFIP added to DCE and monitored the reaction outcomes by ^{1}H NMR. As shown in Figure 5-d, the yields of **4a** and **5a** showed a strong, near-linear correlation with HFIP equivalents. Linear regression for the yield of **4a** gave a Pearson's correlation coefficient of r = -0.966 (R^2 = 0.933), while that for **5a** gave r = +0.968 (R^2 = 0.937). This quantifies the highly predictable nature of the solvent control. Remarkably, the formation of **4a** was nearly undetectable when 9 equiv. of HFIP was added. This indicates that adding 2 drops of HFIP is sufficient to completely switch the product skeleton of this multicomponent reaction (0.2 mmol scale in 2.0 mL solvent). Based on the analysis of the scatter plot (Figure 5-d), we predicted that the reaction would afford approximately equal amounts of **4a** and **5a** upon the addition of 4 equivalents of HFIP. Indeed, when the reaction was scaled up to gram scale, the use of 4 equivalents of HFIP delivered **4a** in 43% yield and **5a** in 39% yield, respectively. The two isomeric products could be readily separated by simple column chromatography. Consequently, our strategy provides a one-pot, parallel access to synthetically valuable (sub-gram) quantities of constitutional isomeric pairs (Figure 5-e). This novel strategy draws an interesting analogy to a classic scenario in asymmetric synthesis: the use of a racemic chiral catalyst gives a racemic product, whereas an enantiopure catalyst delivers the corresponding enantiomerically enriched product. In our system, tuning the loading of HFIP plays an analogous role. Thus, with 0 equiv. of HFIP, the reaction selectively affords a single isomer **4a**; with 9 equivalents, it selectively delivers the other isomer **5a**; and with 4 equivalents, it provides both separable constitutional isomers in nearly equal amounts. This level of synthetic control is difficult to achieve

in other solvent-controlled selective syntheses, which typically require simultaneous variation of multiple parameters such as solvent, additives, and temperature[35, 37].

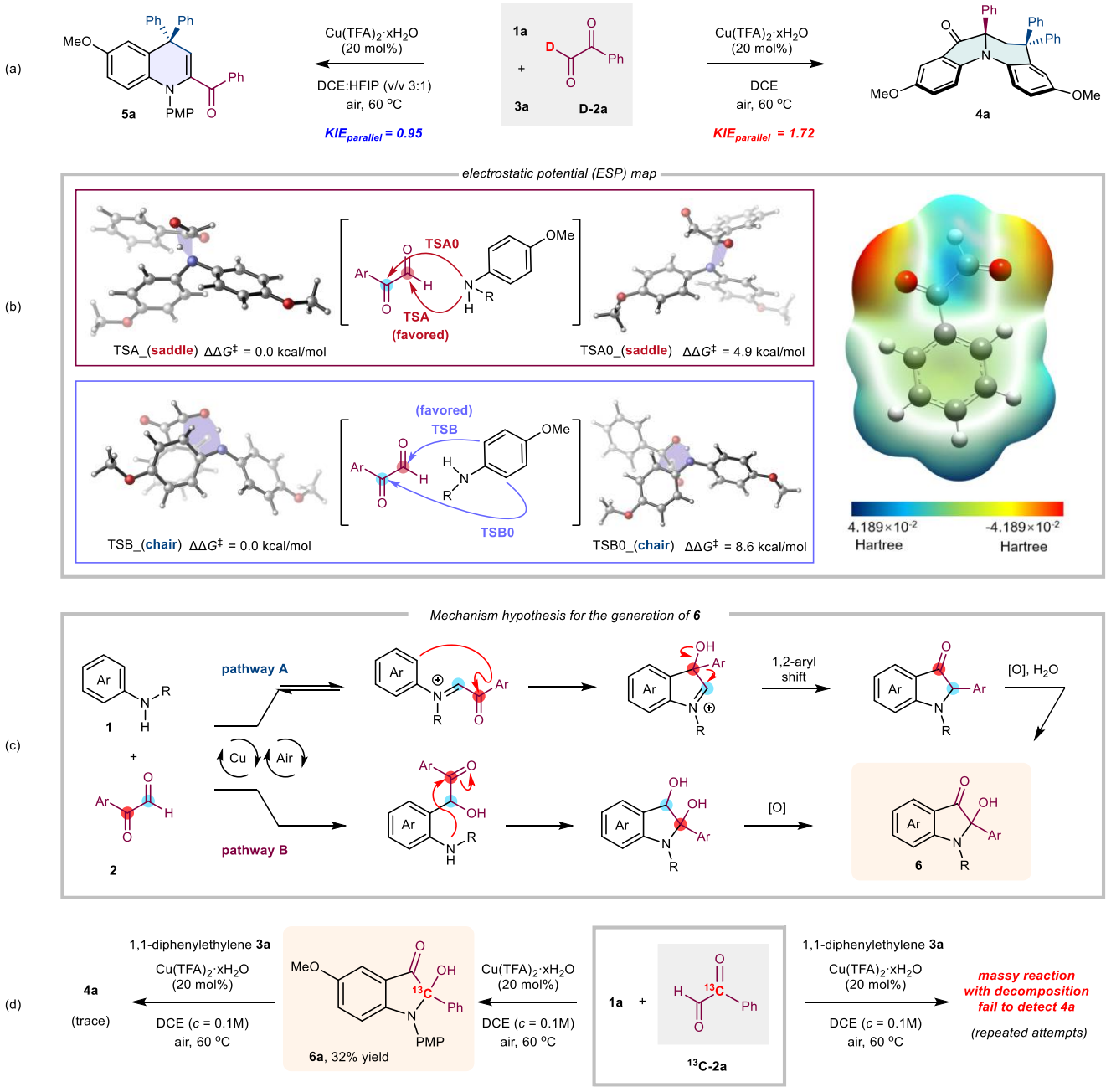


Figure 6 | Mechanistic studies.

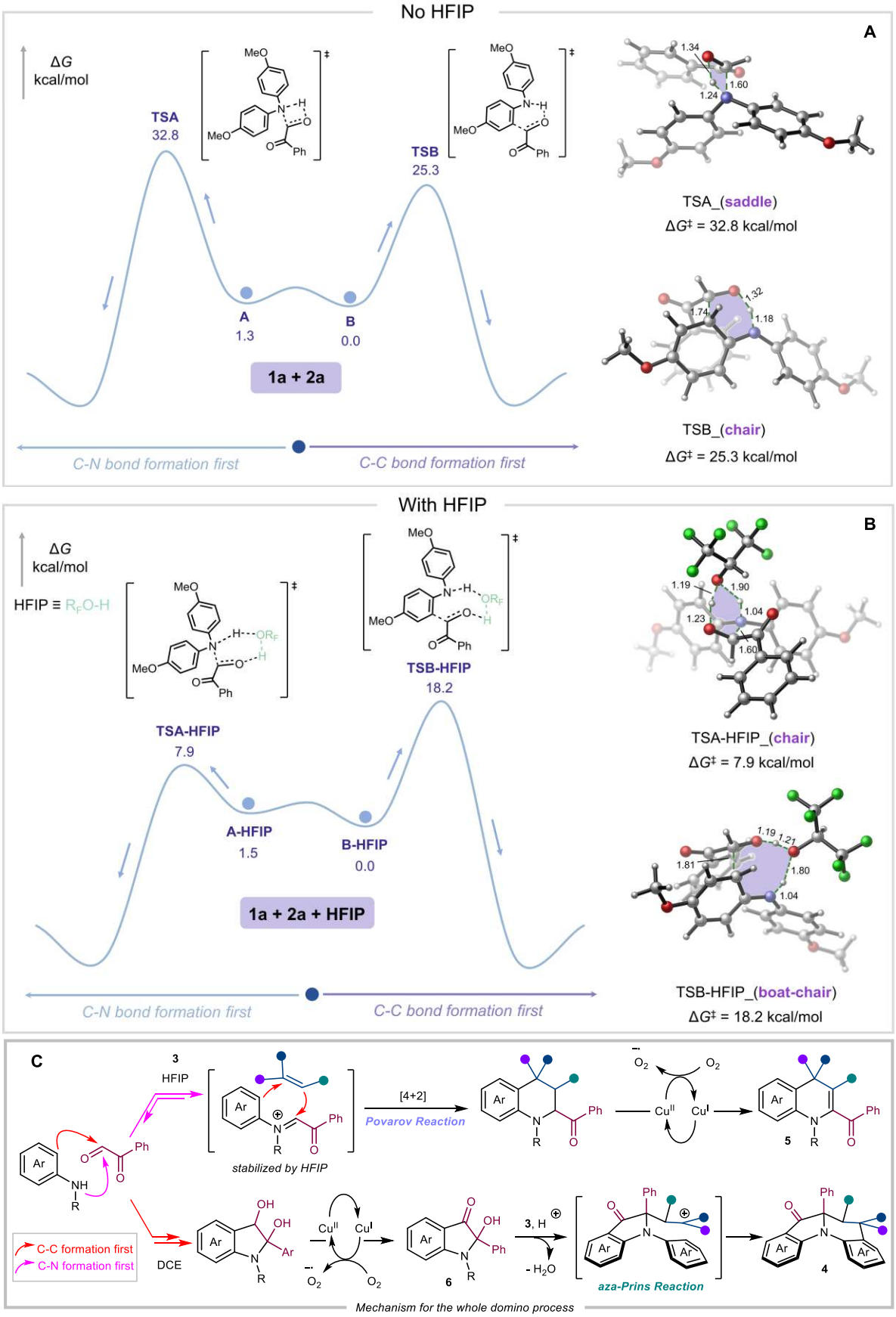


Figure 7 | Calculated Gibbs free energies of the competition between C-N bond formation and C-C bond formation without (A) and with HFIP (B) under Curtin-Hammett conditions at the ωB97XD/def2-TZVPP–SMD(DCE)//B3LYP-D3/def2-SVP–SMD(DCE) level. (All energies are corrected to 333.15 K and 1.0 atm); a plausible reaction mechanism (C).

Next, employing deuterated phenylglyoxal **D-2a** as the substrate, parallel kinetic isotope effect (KIE) experiments[64] were conducted under the respective optimal conditions (Figure 6-a). Those results indicate that for the generation of **4a** (KIE = 1.72), the rate-determining step should precede the formation of the **6** skeletons. Similarly, for the formation of **5a** (KIE = 0.95), the rate-determining step occurs prior to the generation of the intermediate **7a**. These experimental observations suggest that the rate-determining step should occur in the early-stage of the domino sequence, probably associated with the product-determining step[65] in the divergent pathways. Moreover, both the keto and aldehyde carbonyl groups of the arylglyoxals are involved in the formation of **4a**. The electrostatic potential (ESP) map shows that the aldehyde carbonyl is more electrophilic than the keto counterpart (Figure 6b). DFT calculations of the attack of aromatic amines on arylglyoxals further demonstrate that the aldehyde group is energetically favored over the keto carbonyl, regardless of whether the attack occurs via the amino group (C–N bond forming) or via the electron-rich aromatic ring (C–C bond forming), the aldehyde group reacts preferentially over the keto carbonyl group. Furthermore, to investigate whether the formation of **6** involves a 1,2-aryl shift process (Figure 6-b, pathway A vs B),[66-68] isotope labeling experiments were conducted. However, our repeated attempts to use an α-carbonyl ^{13}C-labeled arylglyoxal substrate (**^{13}C-2a**) resulted in a complete failure to form any indolo[1,2-a]quinoline product, yielding instead a messy mixture even with varied reaction temperatures (Figure 6-d, right). Although this anomalous phenomenon has rarely been reported in the literature, we note that ^{12}C/^{13}C substitution can impart a significant primary kinetic isotope effect (KIE) of up to ~8% in a substitution reaction.[69-71] We propose in a multicomponent domino reaction, the magnitude of rate differential can dramatically amplify the selectivity for competing pathways, based on our observation that the reaction outcome is completely altered—rather than merely slowed. We then reacted **^{13}C-2a** with **1a** under the standard conditions. The corresponding product **6a** was obtained in only 32% yield (Figure 6-d, left), in stark contrast to the >90% yield for the transformation in Figure 5-a. Furthermore, using **6a** under the standard conditions failed to afford **4a**, which is also completely different from the transformation shown in Figure 5-a, thereby indicating a pronounced isotopic effect. While this outcome remains to be fully understood and may involve factors other than a ^{12}C/^{13}C KIE, it could be interpreted as preliminary evidence in favor of pathway B.

Our mechanistic studies above reveal that HFIP dictates the chemoselectivity at the early stage of the domino process. Without HFIP, the aryl group preferentially attacks the aldehyde carbonyl to give **4a**, whereas HFIP switches the reaction to *N*-attack, leading to **5a**. This regioselectivity switch—aromatic amine attacking a di-carbonyl electrophile at either the *N* or ortho-*C* site—is a documented but mechanistically unresolved problem.[72, 73] To further reveal the origin of regioselectivity switch triggered by HFIP, DFT calculations regarding the early stage of the domino process with or without HFIP were then performed. Considering the computational error bar associated with conformer choice, all of the selectivity-determining transition states were subjected to thorough conformational searching to locate the lowest-energy conformers.[74] As shown in Figure 7-A, the intermediates of **A** and **B**, composed by **1a** and **2a**, is a pair of conformational isomers that eventually lead to **5a** and **4a** via **TSA** and **TSB** respectively, which is consistent with the Curtin-Hammett principle. In the absence of HFIP, the C–N bond formation proceeds via a four-membered saddle **TSA**, which needs to overcome an activation energy barrier of 32.8 kcal/mol. By comparison, the competing C–C pathway proceeds via a concerted six-membered TSB that adopts a pseudo chair conformation, which requires an activation barrier of 25.3 kcal/mol and is 7.5 kcal/mol lower than the C-N pathway. The DFT calculations regarding the absence of HFIP indicated that the formation of **4a** via C-C pathway is kinetically more favorable, which agrees with the experimental observations.

To further investigate the effect of solvent on regioselectivity, the HFIP molecule was explicitly included in subsequent DFT calculations. In a recent report regarding the reaction between 1,2,4,5-tetrazine and enamine from Houk and co-workers,[75, 76] DFT calculations suggested that the explicit HFIP solvation can lead to unusual cycloadditions and thus provide a lower energy pathway that entirely changes the observed product. As shown in Figure 7-B, it was found that the HFIP could also participate in the present reactions as a strong hydrogen-bond donor,[77, 78] transforms the C-C bond formation step from a chair-like six-membered **TSB** into a boat-chair eight-membered **TSB-HFIP**, which needs to overcome an activation energy barrier of 18.2 kcal/mol to finally give **4a**. In contrast, the engagement of HFIP makes the counterpart C-N bond formation step changing from a rigid four-membered saddle **TSA** into a pseudo six-membered **TSA-HFIP**, which requires a low activation energy barrier of 7.9 kcal/mol. The energetic disparity of 10.3 kcal/mol in activation energy barrier indicates that the C-N bond formation is kinetically more favorable than the competing C-C pathway, which is consistent with the experimental observation that **5a** forms much faster than **4a** with the inclusion of HFIP. To sum up, the current DFT calculations suggested that the addition of HFIP in solvent enables a direct participation of HFIP in selectivity-determining mechanistic steps, which changes the ring size of key transition states. A consequence of that is both C-N bond formation and C-C bond formation are energetically promoted compared to no HFIP conditions. However, the C-N pathway seems to be more sensitive to the participation of HFIP, dramatically lowering the activation energy barrier from 32.8 kcal/mol to 7.9 kcal/mol, while the C-C pathway lowers moderately from 25.3 kcal/mol to 18.2 kcal/mol. This may be due to the ring size change from rigid four-membered **TSA** to flexible six-membered **TSA-HFIP** heavily impact the total activation energy and finally lead to obvious regioselectivity switch. Such solvent-driven selectivity reversal through conformational stabilization of transition states remains rare in the literature and the current work may provide a valuable blueprint for chemodivergence design. Notably, it has been reported that indoline nucleophiles react with *p*-quinone methides to give *C*-alkylation in HFIP as solvent but *N*-alkylation under catalytic HFIP.[79] In our system, the selectivity is completely inverted: *N*-attack prevails with HFIP, whereas *C*-attack dominates in its absence. Our results reveal a new paradigm for HFIP action involving both substrates, although we are fully aware of the differences between the *p*-quinone methides and dicarbonyl electrophiles.

Based on the results, a plausible mechanism is proposed (Figure 7-C). In DCE, the electron-rich arene of **1a** preferentially attacks the aldehyde carbonyl of **2a**, leading to initial C–C bond formation; subsequent copper-catalyzed aerobic oxidation delivers intermediate **6**. In HFIP, the condensation of **1a** and **2a** to form an iminium intermediate becomes operative: HFIP promotes this proton-transfer-mediated step and may stabilize the resulting cation through strong hydrogen-bonding interactions. This early diversion then dictates two separate downstream alkene-capture pathways: one proceeding through an *aza*-Prins reaction to furnish indolo[1,2-*a*]quinolines **4a**, while the other through a Povarov reaction to afford 2-acyl-1,4-dihydroquinolines **5a**, respectively.

Discussion

In summary, we report the first example of solvent-controlled synthesis of two polycyclic constitutional isomers. A minute addition of HFIP to DCE switches the outcome of a mild copper-catalyzed aerobic reaction of readily available diarylamines, arylglyoxals, and alkenes to afford isomeric products indolo[1,2-a]quinolines and 2-acyl-,4-dihydroquinolines, respectively. This work reveals that HFIP, through hydrogen-bonding differentiation of competing transition states, can redirect the inherent selectivity of electron-rich arylamines toward multi-carbonyl electrophiles. By leveraging the classic aza-Prins and Povarov reactions, this domino then orchestrates divergent sequences to

achieve a bifurcation within a single synthetic protocol. Owing to the operational simplicity, paired isomeric products from identical precursors with matched properties are easily obtained, thereby facilitating parallel exploration of their divergent chemical and biological spaces. Biological evaluation against three human cancer cell lines demonstrates that this solvent-switched synthesis directly results in products' bioactivity divergence. We predict that this strategy will serve as an efficient blueprint for diversity-generating synthesis and scaffold hopping research.

Methods

In a 35 mL heavy-wall pressure tube were added 4,4′-dimethoxydiphenylamine **1a** (45.9 mg, 0.2 mmol), phenylglyoxal **2a** (53.7 mg, 0.4 mmol), alkenes **3a** (72.1 mg, 0.4 mmol), $Cu(TFA)_2 \cdot xH_2O$ (12.3 mg, 0.04 mmol) and DCE (2.0 mL, c 0.1 M) or a mixed solvent of DCE and HFIP (2.0 mL, c 0.1 M, v/v 3:1). The resulting mixture was stirred at 60 °C (heating block) for 5 h until substrate conversion was almost complete by TLC analysis. After the reaction was stopped and cooled to room temperature, the reaction mixture was quenched with saturated $NaHCO_3$ solution (50 mL) and NaCl solution (200 mL). The mixture was then extracted with EtOAc (150 mL × 2), and the organic layers were separated and combined. The mixture was dried with anhydrous Na_2SO_4 and concentrated under reduced pressure. The crude product was purified by column chromatography on silica gel (300–400 mesh, eluted with PE : DCM = 3:1) to afford the product **4a** or **5a.**

The crystals were mounted on a glass fiber for diffraction experiments. Intensity data were collected on a Bruker SMART APEX CCD diffractometer with Mo Kα radiation (0.71073 Å) at room temperature.

NMR spectra were recorded on a Bruker Avance III-600 spectrometer at room temperature, ^{1}H frequency is at 600 MHz, and ^{13}C frequency is at 150 MHz. Chemical shifts (δ) were reported in parts per million (ppm) relative to residual solvent peaks rounded to the nearest 0.01 for proton and 0.1 for carbon (*ref: $CDCl_3$ [^{1}H: 0.00 (TMS), ^{13}C: 77.00; DMSO-d_6 [^{1}H: 2.50, ^{13}C: 39.50].* Coupling constants (*J*) were reported in Hz to the nearest 0.1 Hz. Peak multiplicity was indicated as follows s (singlet), d (doublet), t (triplet), q (quartet), m (multiplet), and br (broad). Attribution of peaks was done using the multiplicities and integrals of the peaks.

The accurate masses were measured by the mass spectrometry service using Thermo Scientific LTQ Orbitrap XL.

Data availability. The authors declare that the data supporting the findings of this study are available within the paper and the Supplementary Information, as well as from the authors upon request.

REFERENCES

1. Jurczyk, J.; Woo, J.; Kim, S. F.; Dherange, B. D.; Sarpong, R.; Levin, M. D. Single-atom logic for heterocycle editing. *Nat. Synth.* **2022,** *1*, 352–364.

2. Peplow, M. 'Almost Magical': Chemists Can Now Move Single Atoms in And Out of a Molecule's Core. *Nature* **2023,** *618*, 21-24.

3. Bi, X. H.; Wei, H.; Lu, H. J.; Song, S. Skeletal Editing of Cyclic Scaffolds. *CCS Chem.* **2026,** *8*, 607–692.

4. Ma, C.-H.; Lindsley, C. W.; Chang, J.-B.; Yu, B. Rational Molecular Editing: A New Paradigm in Drug Discovery. *J. Med. Chem.* **2024,** 67, 11459-11466.

5. Li, E.-Q.; Lindsley, C. W.; Chang, J.-B.; Yu, B. Molecular Skeleton Editing for New Drug Discovery. *J. Med. Chem.* **2024,** *67*, 13509-13511.

6. Sun, H. M.; Tawa, G.; Wallqvist, A. Classification of Scaffold-Hopping Approaches. *Drug Discovery Today* **2012,** *17*, 310-324.

7. Callis, T. B.; Garrett, T. R.; Montgomery, A. P.; Danon, J. J.; Kassiou, M. Recent Scaffold Hopping Applications in Central Nervous System Drug Discovery. *J. Med. Chem.* **2022,** *65*, 13483-13504.

8. Acharya, A.; Yadav, M.; Nagpure, M.; Kumaresan, S.; Guchhait, S.K. Molecular Medicinal Insights into Scaffold Hopping-Based Drug Discovery Success. *Drug Discovery Today* **2024,** *29*, 103845.

9. Kovar, O.; Kufa, M.; Finger, V.; Soukup, O.; Kratky, M.; Torruellas, C.; Roh, J.; Korabecny, J. Scaffold Hopping in Tuberculosis Drug Discovery: Principles, Applications, and Case Studies. *J. Med. Chem.* **2025,** *68*, 20903-20929.

10. Stockdale, T. P.; Williams, C. M. Pharmaceuticals that Contain Polycyclic Hydrocarbon Scaffolds. *Chem. Soc. Rev.*, **2015**, *44,* 7737-7763.

11. Shearer, J.; Castro, J. L.; Lawson, A. D. G.; MacCoss, M.; Taylor, R. D. Rings in clinical trials and drugs: Present and future. *J. Med. Chem.* **2022**, *65*, 8699–8712.

12. An example of a polycyclic constitutional isomer exhibiting enhanced biological activity, see: Wang, L., Fang, K., Cheng, J., Li, Y., Huang, Y., Chen, S., Dong, G., Wu S., Sheng, C. Scaffold Hopping of Natural Product Evodiamine: Discovery of a Novel Antitumor Scaffold with Excellent Potency against Colon Cancer. *J. Med. Chem.* **2020**, *63*, 696–713.

13. O' Connor, C. J.; Beckmann, H. S. G.; Spring, D. R. Diversity-oriented Synthesis: Producing Chemical Tools for Dissecting Biology. *Chem. Soc. Rev.* **2012,** *41*, 4444-4456.

14. Galloway, W. R. J. D.; Isidro-Llobet, A.; Spring, D. R. Diversity-oriented Synthesis as a Tool for the Discovery of Novel Biologically Active Small Molecules. *Nat. Commun.* **2010,** *1*, 80.

15. Garcia-Castro, M.; Zimmermann, S., Sankar, M. G.; Kumar, K. Scaffold Diversity Synthesis and Its Application in Probe and Drug Discovery. *Angew. Chem. Int. Ed.* **2016**, *55*, 7586-7605.

16. Tian, Q.-Y.; Ge, J.; Liu, Y.-P.; Wu, X.; Li, Z.-H.; Cheng, G.-L. Solvent-Controlled Enantiodivergent Construction of P (V)- Stereogenic Molecules via Palladium-Catalyzed Annulation of Prochiral N-Aryl Phosphonamides with Aromatic Iodides. *Angew. Chem., Int. Ed.* 2024, *63*, e202409366.

17. Barluenga, J.; Alonso, J.; Fañanás, F. J. Solvent-Controlled Diastereoselective Synthesis of Cyclopentane Derivatives by a [3 + 2] Cyclization Reaction of α,β-Disubstituted (Alkenyl)(Methoxy) Carbene Complexes with Methyl Ketone Lithium Enolates. *J. Am. Chem. Soc.* **2003,** *125*, 2610-2616.

18. Ng, S. M.; Bader, S. J.; Snapper, M. L. Solvent-Controlled Intramolecular [2 + 2] Photocycloadditions of α-Substituted Enones. *J. Am. Chem. Soc.* **2006,** *128*, 7315-7319.

19. Su, Y.-L.; Gao, S.; Huang, Y.; Lin, A.-J.; Yao, H.-Q. Solvent-Controlled C2 / C5-Regiodivergent Alkenylation of Pyrroles. *Chem. Eur. J.* **2015,** *21*, 15820-15825.

20. Wen, K.; Wu, Z.-X.; Huang, B.-R.; Ling, Z.; Gridnev, I. D.; Zhang, W.-B. Solvent-Controlled Pd (II)- Catalyzed Aerobic Chemoselective Intermolecular 1,2-Aminooxygenation and 1,2-Oxyamination of Conjugated Dienes for the Synthesis of Functionalized 1,4-Benzoxazines. *Org. Lett.* **2018,** *20*, 1608-1612.

21. Miao, M.-Z.; Luo, Y.; Xu, H.-P.; Chen, Z.-K.; Xu, J.-F.; Ren, H.-J. Solvent-Controlled, Tunable Hydrosulfonylation of 3-Cyclopropylideneprop-2-en-1-ones. *Org. Lett.* **2016,** *18*, 4292-4295.

22. Dai, H.-M.; Yu, C.; Wang, Z.-H.; Yan, H.; Lu, C.-S. Solvent-Controlled, Tunable β-OAc and β - H Elimination in Rh (III)- Catalyzed Allyl Acetate and Aryl Amide Coupling via C - H Activation. *Org. Lett.* **2016,** *18*, 3410-3413.

23. Giri, R.; Mosiagin, I.; Franzoni, I.; Noetel, N. Y.; Patra, S.; Katayev, D. Photoredox Activation of Anhydrides for the Solvent-Controlled Switchable Synthesis of gem-Difluoro Compounds. *Angew. Chem., Int. Ed.* 2022, *134*, e202209143.

24. Li, H.; Shen, M.-Y.; Li, B.; Zhang, X.-Y.; Fan, X.-S. Solvent-Dependent Selective Synthesis of CF_3-Tethered Indazole Derivatives Based on Multiple Bond Activations. *Org. Lett.* **2023,** *25*, 720-725.

25. Wu, F.-L.; Wang, H.-K.; Wu, Z.-W.; Liu, Y.-B.; Feng, X.-M. Solvent-Controlled Enantioselective Allylic C - H Alkylation of 2,5-Dihydrofuran via Synergistic Palladium / Nickel Catalysis. *J. Am. Chem. Soc.* **2025,** *147*, 16237-16247.

26. Wang, H.-M.; Lu, Q.-Q.; Qian, C.-H.; Liu, C.; Liu, W.; Chen, K.; Lei, A.-W. Solvent-Enabled Radical Selectivities : Controlled Syntheses of Sulfoxides and Sulfides. *Angew. Chem., Int. Ed.* **2016,** *55*, 1094-1097.

27. Li, M.-B.; Grape, E. S.; Backvall, J. E. Palladium-Catalyzed Stereospecific Oxidative Cascade Reaction of Allenes for the Construction of Pyrrole Rings: Control of Reactivity and Selectivity. *ACS Catal.* **2019,** *9*, 5184-5190.

28. Ji, K.; Lu, K.; Huang, J.; Li, Z.-H.; Ke, H.; Chen, Z.-M. Bronsted Acid-Catalyzed Regioselective Hydrothiolation of Dienes: Solvent-Controlled Divergent Synthesis of Sulfides. *Org. Lett.* **2021,** *23*, 8028-8032.

29. Roy, T.; Jana, S.; Das, P. CuF_2 -Catalyzed Chan - Lam Reaction of Saccharin: Solvent-Controlled Chemodivergent Synthesis of N - Arylsaccharin and Methyl 2-(N-Arylsulfamoyl)benzoates. *J. Org. Chem.* **2025,** *90*, 9083-9097.

30. Yang, T.; Ma, Z.-G.; Zhang, W.-H.; Shan, Z.-N.; Zhou, Y.; Zhang, L.-Y.; Lei, C.-W. MgI_2-Mediated Solvent-Controlled Divergent Ring-Opening Cyclization / Addition of Spirocyclopropyl Indanediones. *J. Org. Chem.* **2025,** *90*, 16833-16844.

31. He, J.-X.; Zhang, Z.-H.; Mu, B.-S.; Cui, X.-Y.; Zhou, J.; Yu, J.-S. Catalyst-Free and Solvent-Controlled Divergent Synthesis of Difluoromethylene-Containing S -Heterocycles. *J. Org. Chem.* **2021,** *86,* 9206-9217.

32. Li, R.; Hou, Y.-X.; Xu, J.-H.; Gao, Y.; Hu, X.-Q. Divergent Synthesis of Fused N-heterocycles via Rhodium-Catalysed [4 + 2] Cyclization of Pyrazolidinones with Iodonium Ylides. *Org. Chem. Front.* **2022,** *9*, 2181-2186.

33. Hazra, S.; Hirano, K.; Miura, M. Solvent-Controlled Rhodium-Catalyzed C6-Selective C. *Asian J. Org. Chem.* **2019***, 8,* 1097–1101.

34. For a selected example, see: Zhu, Z.-X.; Glinkerman, C. M.; Boger, D. L. Selective N1 / N4 1,4-Cycloaddition of 1,2,4,5-Tetrazines Enabled by Solvent Hydrogen Bonding. *J. Am. Chem. Soc.* **2020,** 142, 20778-20787.

35. Barluenga, J.; López, S.; Flórez, J. [3+2] and [4+1] Cycloaddition Reactions of Fischer Alkoxy (alkenyl)carbene Complexes with Electronically Neutral 1,3-dienes. *Angew. Chem., Int, Ed.* **2003,** *42*, 231-233.

36. Dörwald, F. Z., Solvent-controlled selectivity in the synthesis of five-membered carbocycles from carbene complexes. *Angew. Chem., Int. Ed.* **2003,** *42*, 1332-1334.

37. Roure, B., Alonso, M., Lonardi, G.; Yildiz, D. B., Buettner, C. S.; Santos, T.; Xu, Y; Bossart, M.; Derdau, V.; Méndez, M.; Llaveria, J.; Ruffoni, A. Leonori, D. *Photochemical permutation of thiazoles, isothiazoles and other azoles. Nature* **2025,** *637,* 860–867*.*

38. Zhou, Y.; Lei, S.-G.; Abudureheman, B.; Wang, L.-S.; Yu, Z.-C.; Xiang, J.-C.; Wu, A.-X. Transforming an Azaarene into the Spine of Fusedbicyclics via Cycloaddition-Induced Scaffold Hopping of 5-Hydroxypyrazoles. *Nat. Commun.* **2024,** 15, 10907.

39.Trowbridge, A.; Reich, D.; Gaunt, M. J. “Multicomponent Synthesis of Tertiary Alkylamines by Photocatalytic Olefin-Hydroaminoalkylation,” *Nature* 2018, 561, 522-527.

40. Magolan, J.; Carson, C. A.; Kerr, M. A. Total Synthesis of (±)- Mersicarpine. *Org. Lett.* **2008,** *10*, 1437-1440.

41. Beemelmanns, C.; Gross, S.; Reissig, H. U. Towards the Core Structure of Strychnos Alkaloids Using Samarium Diiodide-Induced Reactions of Indole Derivatives. *Chem. Eur. J.* **2013,** *19*, 17801-17808.

42. Goldbrunner, M.; Loidl, G.; Polossek, T.; Mannschreck, A.; VonAngerer, E. Inhibition of Tubulin Polymerization by 5,6-Dihydroindolo[2,1-a]isoquinoline Derivatives. *J. Med. Chem.* **1997,** *40*, 3524-3533.
43. Ambros. R.; Schneider. M. R.; Angerer. S. V., Indolo[2,1-a]isoquinolines. Syntheses, steroid hormone receptor binding affinities, and cytostatic activity. *J. Med. Chem.* **1990**, *33*, 153-160.
44. Ahmed, E.; Briseno, A. L.; Xia, Y.; Jenekhe, S. A. High Mobility Single-Crystal Field-Effect Transistors from bisindoloquinoline semiconductors. *J. Am. Chem. Soc.* **2008,** *130*, 1118-1119.
45. Sun, K.; Zhang, Y.-L.; Chen, X.-L.; Su, H.-F.; Peng, Q.-C.; Yu, B.; Qu, L.-B.; Li, K. A Type of Atypical AIEgen Used for One-Photon/Two-Photon Targeted Imaging in Live Cells. *ACS Appl. Bio Mater.* **2019,** *3*, 505-511.
46. Zhu, L.-Y.; Kim, E. G.; Yi, Y.-P.; Ahmed, E.; Jenekhe, S. A.; Coropceanu, V.; Bredas, J. L. Charge-Transport Properties of the Tetraphenylbis (indolo [1, 2 - a]) quinoline and 5,7-Diphenylindolo[1,2- a]quinoline Crystals. *J. Phys. Chem. C.* **2010,** *114*, 20401-20409.
47. Li, J.-S.; Liu, Y.-J.; Li, S.; Ma, J.-A. Chiral Phosphoric Acid-Catalyzed Direct Asymmetric Mannich Reaction of Cyclic C - Acylimines with Simple Ketones: Facile Access to C2-Quaternary Indolin-3-Ones. *Chem. Commun.* **2018,** *54*, 9151-9154.
48. Uppalabat, T.; Hassa, N.; Sawektreeratana, N.; Leowanawat, P.; Janthakit, P.; Nalaoh, P.; Promarak, V.; Soorukram, D.; Reutrakul, V.; Kuhakarn, C. Cascade Oxidative Trifluoromethylthiolation and Cyclization of 3-Alkyl-1 -(2-(alkynyl)phenyl) indoles. *J. Org. Chem.* **2023,** *88*, 5403-5419.
49. Hazra, S.; Mondal, B.; De, R. N.; Roy, B. Pd-Catalyzed Dehydrogenative C - H Activation of Iminyl Hydrogen with the Indole C3 - H and C2 - H Bond: An Elegant Synthesis of Indeno[1,2- b]indoles and Indolo[1,2- a] indoles. *RSC Adv.* **2015,** *5*, 22480-22489.
50. Wu, X.-P.; Xiao, Y.; Sun, S.; Yu, J.-T.; Cheng, J. Rhodium-Catalyzed Reaction of Sulfoxonium Ylides and Anthranils toward Indoloindolones via a (4 + 1) Annulation. *Org. Lett.* **2019,** *21*, 6653-6657.
51. Zhao, Y.-L.; Li, S.; Fan, Y.-H.; Guo, X.-Q.; Jiao, X.; Tian, L.-J.; Sun, X.-J. Synthesis of 10 *H* -Indolo[1,2- a]indole Derivatives via Intramolecular Cycloaddition and H-Migration. *Eur. J. Org. Chem.* **2021,** *2021*, 4358-4363.
52. Jeedimalla, N.; Flint, M.; Smith, L.; Haces, A.; Minond, D.; Roche, S. P. Multicomponent Assembly of 4-Aza-Podophyllotoxins: A Fast Entry to Highly Selective and Potent Anti-Leukemic Agents. *Eur. J. Med. Chem.* **2015,** *106*, 167-179.
53. Ţînţaş, M.-L.; Peauger, L.; Alix, F.; Papamicaël, C.; Besson, T.; Sopková-de Oliveira Santos, J.; Gembus, V.; Levacher, V. Straightforward Access to a New Class of Dual DYRK1A/CLK1 Inhibitors Possessing a Simple Dihydroquinoline Core, *Molecules* **2023**, *28*, 36.
54. Wang, D.; Jiang, Y.-Y.; Dong, L.-R.; Li, G.-Y.; Sun, B.-Y.; Desaubry, L.; Yu, P. One-Pot Selective Saturation and Functionalization of Heteroaromatics Leading to Dihydropyridines and Dihydroquinolines. *J. Org. Chem.* **2020,** *85*, 5027-5037.
55. Diaba, F.; Le Houerou, C.; Grignon-Dubois, M.; Gerval, P. Organosilicon Entry to the Regioselective Cyanomethylation of Quinolinium Methiodides. *J. Org. Chem.* **2000,** *65*, 907-910.
56. Watanabe, Y.; Yamamoto, T.; Ozaki, S. Regiospecific Synthesis of 2,6-di-O (Alpha-D-Mannopyranosyl) Phosphatidyl-D-Myo - Inositol. *J. Org. Chem.* **1996,** *61*, 14-15.
57. Chen, Q.; Zhang, S.-W.; Zhang, T.; He, K.-X.; Yuan, Y.; Jia, X.-D. Radical C-H Bond Oxidation Initiated Intramolecular Cyclization of Glycine Esters: Construction of Dihydroquinoline Skeletons. *Asian J. Org. Chem.* **2019,** 8, 115-118.

58. Bohn, P.; Le Fur, N.; Hagues, G.; Costentin, J.; Torquet, N.; Papamicael, C.; Marsais, F.; Levacher, V. Rational Design of Central Selective Acetylcholinesterase Inhibitors by Means of A " Bio-Oxidisable Prodrug " Strategy. *Org. Biomol. Chem.* **2009,** *7*, 2612-2618.

59. Wu, X.-J.; Jiang, R.; Wu, B.; Su, X.-M.; Xu, X.-P.; Ji, S.-J. Nano-Iron Oxide as a Recyclable Catalyst for Intramolecular C - N Cross-Coupling Reactions under Ligand-Free Conditions: One-Pot Synthesis of 1,4-Dihydroquinoline Derivatives. *Adv. Synth. Catal.* **2009,** *351*, 3150-3156.

60. Su, Y.-C; Zhang, S.-W.; Yuan, Y.; Ma, Q.-Y.; Sun, Z.; Yuan, Y.; Jia, X.-D. $SbCl_3$ Initiated Conjunctive C - H Bond Functionalization and Carbochlorination between Glycine Esters and Methylenecyclopropanes (MCPs). *Chem. Commun.* **2021,** *57*, 9878-9881.

61. Liao, M.-L.; Guo, Q.; Ao, Y.; Yang, J.-C.; Li, P.-G.; Zou, L.-H. Solvent-Controlled [4 + 2] Annulation Reaction: Selective Synthesis of 1,4-Dihydroquinolines / Quinolines. *J. Org. Chem.* **2026,** *91*, 1215-1222.

62. Allen, S. E.; Walvoord, R. R.; Padilla-Salinas, R.; Kozlowski, M. C. Aerobic Copper-Catalyzed Organic Reactions. *Chem. Rev.* **2013,** *113*, 6234-6458.

63. McCann, S. D.; Stahl, S. S. Copper-Catalyzed Aerobic Oxidations of Organic Molecules: Pathways for Two-Electron Oxidation with a Four-Electron Oxidant and a One-Electron Redox-Active Catalyst. *Acc. Chem. Res.* **2015,** *48*, 1756-1766.

64. Simmons, E. M.; Hartwig, J. F. On the Interpretation of Deuterium Kinetic Isotope Effects in C-H Bond Functionalizations by Transition-Metal Complexes. *Angew. Chem., Int, Ed.* **2012,** 51, 3066-3072.

65. The definition of “product-determining step” in IUPAC Gold book (http://old.iupac.org/goldbook/P04862.pdf) is as follows: “The step of a stepwise reaction, in which the product distribution is determined. The product-determining step may be identical to, or occur later than, the rate-controlling step on the reaction coordinate.”

66. He, Y.-P.; Wu, H.; Wang, Q.; Zhu, J.-P. Catalytic Enantioselective Synthesis of Morpholinones Enabled by Aza-Benzilic Ester Rearrangement. *J. Am. Chem. Soc.* **2021,** *143*, 7320-7325.

67. Li, X.-Z.; He, Y.-P.; Wu, H. Zinc Chloride-Catalyzed Cyclizative 1,2-Rearrangement Enables Facile Access to Morpholinones Bearing Aza-Quaternary Carbons. *Commun. Chem.* **2023,** 6, 216.

68. He, Y.-P.; Quan, R.; Li, X.-Z.; Zhu, J.-P.; Wu, H. Asymmetric Construction of α,α-Disubstituted Piperazinones Enabled by Benzilic Amide Rearrangement. *Angew. Chem., Int. Ed.* **2023,** *62*, e202217954.

69. Matsson, O.; Dybala-Defratyka, A.; Rostkowski, M.; Paneth, P.; Westaway, K. C. A Theoretical Investigation of α-Carbon Kinetic Isotope Effects and Their Relationship to the Transition-State Structure of S_N2 Reactions. *J. Org. Chem.* **2005,** *70*, 4022-4027.

70. Sicinska, D.; Truhlar, D. G.; Paneth, P. Dependence of Transition State Structure on Substrate: The Intrinsic C-13 Kinetic Isotope Effect Is Different for Physiological and Slow Substrates of the Ornithine Decarboxylase Reaction Because of Different Hydrogen Bonding Structures. *J. Am. Chem. Soc.* **2005,** *127*, 5414-5422.

71. Singleton, D. A.; Wang, Z.-H. Isotope Effects and the Nature of Enantioselectivity in the Shi Epoxidation. The importance of asynchronicity. *J. Am. Chem. Soc.* **2005,** *127*, 6679-6685.

72. Wang, Y.; Li, Y.-Y.; Chen, H.-H.; Lan, Y.; Pi, C.; Wu, Y.-J.; Cui, X.-L. Enantioselective De Novo Construction of 3 - Oxindoles via Organocatalyzed Formal [3 + 2] Annulation from Simple Arylamines. *Nat. Commun.* **2024,** *15*, 6183.

73. Quan, R.; Li, X.-Z.; Wang, Z.-Q.; He, Y.-P.; Wu, H. Catalytic Asymmetric Cyclizative Rearrangement of Anilines and Vicinal Diketones to Access 2,2-Disubstituted Indolin-3-ones. *Adv. Sci.* **2024,** 11, 2402532.

74. Peng, J.; Chen, L.; Zhu, M.; Sun, L.; Zeng, Z.; Liu, Z. Overcoming Conformational Complexity to Elucidate Selective Ethylene Tetramerization Behavior. *ACS Catal.* **2025**, *15*, 8954-8965.

75. Ma, P.-C.; Svatunek, D.; Zhu, Z.-X.; Boger, D. L.; Duan, X.-H.; Houk, K. N. Computational Studies of Reactions of 1,2,4,5-Tetrazines with Enamines in MeOH and HFIP. *J. Am. Chem. Soc.* **2024,** *146*, 18706-18713.
76. Yang, Y.-F.; Yu, P.-Y.; Houk, K. N. Computational Exploration of Concerted and Zwitterionic Mechanisms of Diels - Alder Reactions between 1,2,3-Triazines and Enamines and Acceleration by Hydrogen-Bonding Solvents. *J. Am. Chem. Soc.* **2017,** *139*, 18213-18221.
77. Motiwala, H. F.; Armaly, A. M.; Cacioppo, J. G.; Coombs, T. C.; Koehn, K R. K. Norwood IV, V. M.; Aubé, J. HFIP in Organic Synthesis. *Chem. Rev*. **2022,** *122*, 12544-12747.
78. Colomer, I.; Chamberlain, A. E. R.; Haughey, M. B.; Donohoe, T. J. Hexafluoroisopropanol as a Highly Versatile Solvent. *Nat. Rev. Chem*. **2017**, *1*, 0088.
79. Akyildiz, V.; Lafzi, F. Kilic, H.; Saracoglu, N. Solvent-controlled regioselective C(5)–H/N(1)–H bond alkylations of indolines and C(6)–H bond alkylations of 1,2,3,4-tetrahydroquinolines with para-quinone methides. *Org. Biomol. Chem.*, **2022**, *20*, 3570–3588.

Supplementary Information is available in the online version of the paper.

Acknowledgment. This work was supported by the National Natural Science Foundation of China (Grant No. 22301035, 22571111, 32370063). This work was also supported by Jiangsu Province Youth Science and Technology Talent Support Project (JSTJ-2024-454), the Fundamental Research Funds for the Central Universities and Southeast University's "Zhi-Shan Young Scholars of Excellence" Support Program (2242025RCB0021), Chengdu Guibao Science & Technology Co., Ltd and the 111 Project B17019 and Big Data Computing Center of Southeast University.

Author Contributions.

J.-C.X., A.-X.W., Z.-X.L. conceived and designed the experiments. T.L., C.-S.Xu., Y.-L.L., J.-C.H., T.-Y.Z., M.Z., Z.-R.C., Y.-T.D. carried out the experiments. J.-C.X., A.-X.W., interpreted the results and co-wrote the manuscript.

Competing interests: The authors declare no competing interests.

Reprints and permission information is available online at http://npg.nature.com/

Supplementary Files

This is a list of supplementary files associated with this preprint. Click to download.

- SupportingInformationforNCV1110.pdf
- TOC.docx